Dysregulated assembly of elastic fibers in fibulin-5 knockout mice results in a tendon-specific increase in elastic modulus

Jeremy D. Eekhoff [a], Heiko Steenbock [b], Ian M. Berke [a], Jürgen Brinckmann [b,c], Hiromi Yanagisawa [d], Jessica E. Wagenseil [e], Spencer P. Lake [a,e,f,*]

[a] Department of Biomedical Engineering, Washington University in St. Louis, USA
[b] Institute of Virology and Cell Biology, University of Lübeck, Germany
[c] Department of Dermatology, University of Lübeck, Germany
[d] Life Science Center for Survival Dynamics, Tsukuba Advanced Research Alliance, University of Tsukuba, Japan
[e] Department of Mechanical Engineering and Materials Science, Washington University in St. Louis, USA
[f] Department of Orthopaedic Surgery, Washington University in St. Louis, USA

ARTICLE INFO

ABSTRACT

Elastic fiber assembly is coordinated in part by fibulin-5, a matricellular protein. When fibulin-5 is not available to guide elastogenesis, elastin forms into disconnected globules instead of the dense elastic fiber core found in healthy tissues. Despite the growing evidence for a significant role of elastic fibers in tendon mechanics and the clinical relevance to cutis laxa, a human disease which can be caused by a mutation in the gene encoding fibulin-5, it is unknown how malformed elastic fibers affect tendon function. Therefore, this study investigated the effects of dysregulated elastic fiber assembly in tendons from fibulin-5 knockout mice in comparison to wild-type controls. Due to evidence for a more prominent role of elastic fibers in tendons with higher functional demands, both the energy-storing Achilles tendon and the more positional tibialis anterior tendon were evaluated. The linear modulus of knockout Achilles tendons was increased compared to controls, yet there was no discernible change in mechanical properties of the tibialis anterior tendon across genotypes. Transmission electron microscopy confirmed the presence of malformed elastic fibers in knockout tendons while no other changes to tendon composition or structure were found. The mechanism behind the increase in linear modulus in fibulin-5 knockout Achilles tendons may be greater collagen engagement due to decreased regulation of strain-induced structural reorganization. These findings support the theory of a significant, functionally distinct role of elastic fibers in tendon mechanics.

1. Introduction

Fibulin-5 is a key matricellular protein involved in the assembly of elastic fibers, a structural component of the extracellular matrix (ECM) of many tissues (Papke and Yanagisawa, 2014; Yanagisawa and Davis, 2010). Elastic fibers are composed of a scaffold of fibrillin-rich microfibrils with dense, highly cross-linked elastin located within the scaffold to impart mechanical elasticity and fatigue resistance (Baldwin et al., 2013; Gosline et al., 2002). While the precise details of the actions of fibulin-5 have yet to be fully understood, proposed roles for the protein include regulating the coacervation of tropoelastin, activation of lysyl oxidase-like 1, and deposition of tropoelastin onto the microfibrillar scaffold (Katsuta et al., 2008; Liu et al., 2004; Freeman et al., 2005). In

humans, mutations in the gene for fibulin-5 can cause a form of cutis laxa, a disease characterized by loose skin and other pathologies including joint laxity, which is indicative of compromised mechanical properties of joint tissues including tendons and ligaments (Sakati et al., 1983; Hu et al., 2006; Berk et al., 2012). Therefore, the pathology of cutis laxa highlights the importance of properly formed elastic fibers in maintaining the mechanics of connective soft tissue.

Fibulin-5 knockout ($Fbln5^{-/-}$) mice have been used as a model of cutis laxa and more generally to explore the effects of malformed elastic fibers (Yanagisawa et al., 2002; Nakamura et al., 2002). Without fibulin-5 to guide elastogenesis, disconnected elastin globules have been observed to take the place of properly formed elastic fibers in the vasculature and skin of this murine model (Yanagisawa et al., 2002;

Nakamura et al., 2002; Choi et al., 2009). Similarly, disconnected malformed elastic fibers have been seen in tissue biopsies from cutis laxa patients (Marchase et al., 1980; Holbrook and Byers, 1982). Notable phenotypes of the *Fbln5$^{-/-}$* mouse mirror those of cutis laxa and include loose skin, tortuous aortae, emphysema, and pelvic organ prolapse (Yanagisawa et al., 2002; Nakamura et al., 2002; Drewes et al., 2007). However, despite the described joint laxity in patients with cutis laxa, there have yet to be any published studies investigating how dysregulated elastic fiber assembly may affect tendons or ligaments using the *Fbln5$^{-/-}$* model.

Moreover, the growing amount of literature on the role of elastic fibers in tendon mechanics further establishes the need to ascertain how malformed elastic fibers resulting from fibulin-5 deficiency affect tendon function (Hill et al., 2020). Research using elastase to degrade elastin in human palmaris tendon and supraspinatus tendon, porcine medial collateral ligament, and rat tail tendon fascicles has demonstrated that the loss of elastin in otherwise healthy tendon alters the mechanical properties, although the precise roles and mechanisms of elastic fibers in tendon and ligament remain unclear due to some conflicting results (Henninger et al., 2013, 2015; Millesi et al., 1995; Fang and Lake, 2016; Grant et al., 2015). While enzyme-based approaches can provide useful insights, such studies can be subject to limitations including proteolytic non-specificity and limited enzyme penetration. Elastinopathic murine models represent one alternate approach to overcome such limitations and target specific components of elastic fibers; our recent work demonstrated that tendons from elastin haploinsufficient mice had increased stiffness compared to wild-type controls (Eekhoff et al., 2017).

In addition, the relative importance of elastic fibers in tendon is likely to vary according to the specific function of each particular tendon. For example, the greater elastin content in the equine superficial digital flexor tendon (SDFT) compared to the common digital extensor tendon (CDET) seems likely to contribute to greater extensibility and fatigue resistance of the SDFT (Godinho et al., 2017; Thorpe et al., 2012, 2017). These mechanical differences, in turn, are uniquely suited to the functional requirement of the SDFT to store and release mechanical energy and withstand frequent high strain loading during the gait cycle (Alexander, 1991; Thorpe et al., 2015). Tendons with similar functions in other species, such as the Achilles tendon in humans or in mice, are expected to have similar relationships between ECM composition, mechanical properties, and functional requirements.

Elastic fibers have been theorized to contribute to tendon mechanics by acting as linking components between adjacent bundles of collagen (Henninger et al., 2013; Eekhoff et al., 2017). In this capacity, they may regulate structural reorganization mechanisms (e.g., collagen sliding and rotation) when tendons are loaded (Fang and Lake, 2015). Additionally, elastic fibers appear to have distinct roles depending on their location within the tendon. Elastic fibers within collagen fascicles are sparse and strongly aligned with the collagen, while elastic fibers between fascicles in the interfascicular matrix form a more dense, mesh-like network (Godinho et al., 2017; Pang et al., 2017; Grant et al., 2013). In larger tendons with a distinct fascicular structure it is difficult to distinguish the differential contribution of fascicular and interfascicular elastic fibers, necessitating simpler models to isolate the effects of each. Due to its small size, murine tendon structurally resembles a single fascicle from a larger tendon and does not contain interfascicular matrix, making it an ideal model to isolate and evaluate how elastic fibers function within tendon fascicles (Lee and Elliott, 2019a).

Therefore, the objective of this study was to determine how fibulin-5 deficiency affects functionally distinct tendons in the *Fbln5$^{-/-}$* model. We investigated two tendons from the murine hindlimb: the Achilles tendon (AT), which is cyclically loaded to high strains and stores mechanical energy, and the tibialis anterior tendon (TBAT), which experiences lower magnitude strain and helps to stabilize the joint. Informed by our prior work with elastin haploinsufficient mice and the different functional requirements of the AT and TBAT, we hypothesized that the

tendons from *Fbln5$^{-/-}$* mice would have a greater elastic modulus compared to controls due to structurally unsound elastic fibers, and that the effect would be greater in the AT compared to the TBAT.

2. Methods

2.1. Sample acquisition and preparation

Achilles tendons (ATs) and tibialis anterior tendons (TBATs) were harvested from male fibulin-5 knockout (*Fbln5$^{-/-}$*) and wild-type (*Fbln5$^{+/+}$*) mice between four and five months of age after euthanization (Budatha et al., 2011). Tendons appointed for mechanical testing and compositional analysis were wrapped in phosphate buffered saline (PBS)-soaked gauze and stored at -20 °C until further use, while tendons utilized for two-photon microscopy or transmission electron microscopy were immediately processed following euthanization and tissue collection, as described below. All experiments were performed with approval from the Institutional Animal Care and Use Committee.

2.2. Compositional analysis

Desmosine, a cross-link specific to elastin, and hydroxyproline, a post-translationally modified amino acid which is largely specific to collagen, were quantified in ATs and TBATs using amino-acid based biochemical assays in triplicate on a single 96-well plate to reduce plate-to-plate variability (n = 6/group) (Stoilov et al., 2018). Tendon dry weight was measured after lyophilizing the samples for 24 h. Next, the samples were hydrolyzed in 6 N HCl at 100 °C for 48 h. Following hydrolysis, HCl was evaporated off and the samples were rehydrated in ultrapure water to a final concentration of 5 µg of sample dry weight per microliter of water.

Desmosine quantity was determined using a competitive enzyme-linked immunosorbent assay (Stoilov et al., 2018). A 96-well plate was coated for 30 min with desmosine-ovalbumin conjugate in 50 mM carbonate/bicarbonate buffer (pH 9.6), and then blocked for 15 min using blocking buffer. After washing the wells with wash solution (KPL 506300), the hydrolyzed samples or an elastin standard were added to each well with desmosine antibody in blocking solution (KPL 506100) for 60 min, followed by an additional wash. Then, peroxidase-labeled antirabbit IgG in blocking solution was added as the secondary antibody for 60 min. After a final wash, a peroxidase substrate was added to induce a colorimetric change. Absorbance was measured at 650 nm at 20 min after the addition of the peroxidase substrate. A standard curve was produced using the same procedure on purified bovine elastin, which contains 3.4 ng of desmosine per microgram of elastin (Stoilov et al., 2018). No assumptions were made regarding desmosine to elastin ratio in the tendon samples, due to the potential for altered cross-linking capabilities in the *Fbln5$^{-/-}$* tissue.

Hydroxyproline content was measured using a colorimetric chloramine-T based assay (Stoilov et al., 2018). Sample hydrolysates were oxidized with 15.8 mg/mL Chloramine-T in n-propanol and citrate acetate buffer (pH 6.5) and subsequently reacted with Erlich's solution (190 mg/mL p-dimethylaminobenzaldehyde in n-propanol and perchloric acid) to induce a colorimetric change. Absorbance at 550 nm was measured after heating to 65 °C for 30 min. Pure hydroxyproline was used for the standard curve, and hydroxyproline values were converted to collagen by assuming collagen was made up of 13.5% hydroxyproline in both the standard and in the samples (Stoilov et al., 2018). This assumption was made because previous data shows that fibulin-5 does not disrupt collagen synthesis, which includes hydroxylation of proline residues within the collagen α-chains (Yanagisawa et al., 2009).

In separate samples, collagen cross-links were measured using amino acid analysis (n = 5–6/group) (Dunham et al., 2020). Due to the small size of the murine TBATs, tendons from paired limbs were pooled together for analysis, while ATs were large enough to be analyzed

individually. Samples were reduced by 25 mg/mL sodium borohydride sodium biphosphate buffer (pH 7.4) to stabilize acid-labile collagen cross-links, followed by hydrolysis in 6 N HCl at 110 °C for 24 h. The hydrolyzates were precleared by solid phase extraction to remove the majority of non-crosslinked amino acids. Dried eluates were redissolved in sodium citrate loading buffer (pH 2.2) and analyzed on an amino acid analyzer using a three-buffer gradient system and post column ninhydrin derivatization. The column was eluted for 5 min (flow rate 15 ml/h) with sodium citrate buffer (pH 4.25), then for 40 min with sodium citrate buffer (pH 5.35) and then for 20 min with sodium citrate/borate buffer (pH 8.6) at 80 °C. Retention times of individual cross-links were established with authentic cross-link compounds. Quantitation was based on ninhydrin generated leucine equivalence factors (dihydroxylysinonorleucine [DHLNL] and hydroxylysinonorleucine [HLNL] = 1.8; hydroxylysyl pyridinoline [HP] and lysyl pyridinoline [LP] = 1.7). (Avery et al., 2009).

2.3. Two-photon microscopy

To increase light penetration and, correspondingly, imaging depth, ATs and TBATs were optically cleared using a method adapted from the SeeDB technique (Ke et al., 2013). Freshly harvested whole tendons (n = 4/group) were incubated in 1% Triton-X in 0.1X PBS for one hour to lyse the cells and reduce intracellular autofluorescence, and subsequently were incubated in 0.1X PBS for one hour to wash the Triton-X from the samples. Then, tendons were incubated in serially increasing fructose solutions in 0.1X PBS with the addition of 0.5% thioglycerol to prevent glycation. For the serial incubation, samples were incubated for 2 h in 30% (wt/vol) fructose, 2 h in 60% (wt/vol) fructose, and then moved to 90% (wt/vol) fructose for between 16 and 24 h before being imaged.

Cleared ATs and TBATs were imaged using a two-photon microscope (Olympus FV1000MPE), where the fluorescent signal was collected at 25X (XLPLN25XWMP2, NA 1.05). Collagen signal was acquired using second-harmonic generation (excitation 840 nm; emission 420–460 nm) and elastin signal was acquired using two-photon excited autofluorescence (excitation 840 nm; emission 495–540 nm). Image stacks were taken at 1024 × 1024 resolution with a z-step size of 1 μm through the full depth of the midsubstance of the tendon (300–400 μm).

Elastic fibers were segmented from the background autofluorescent signal. After initial noise reduction using a cubic Gaussian smoothing kernel with a standard deviation of 0.5 voxels, the background signal was isolated by performing a 7 × 7 × 7 voxel median filter on the image stack, effectively removing all elastic fibers from the image. The background was subtracted from the original image stack, and the resultant stack was binarized using an intensity threshold equal to eight times the seventy-fifth percentile of the intensity of all voxels in the resultant image stack. This threshold accounts for variation in overall intensity between images and was effective in preliminary testing. Then all objects smaller than 100 voxels were deleted from the binarized image to remove residual noise. Lastly, the binary mask was applied to the original image to isolate the elastic fibers. The volume of elastin was determined from the binary mask and normalized to collagen volume determined from the second-harmonic generation image.

2.4. Transmission electron microscopy

Transmission electron microscopy (TEM) was used to visualize the nanostructure of elastic fibers within the tendons (n = 2/group). Freshly harvested whole ATs and TBATs were fixed in 2.5% glutaraldehyde and 2% paraformaldehyde overnight at 4 °C and post-fixed in 1.25% osmium tetroxide. After fixation, samples were stained *en bloc* using 2% tannic acid and 4% aqueous uranyl acetate, dehydrated, and embedded in resin. Ultra-thin sections (100 nm) were taken in both the transverse and longitudinal directions from each sample and counterstained using uranyl acetate and lead citrate. Sections were surveyed using a

transmission electron microscope (JEOL JEM-1400) to locate and acquire images of elastic fibers. A minimum of 19 images were taken from the midsubstance each sample at various magnifications and examined to assess elastic fiber structure. Of these, five images of transverse sections from each sample were chosen at random to measure collagen fibril diameters (Eekhoff et al., 2017). Images were manually thresholded and subjected to a watershed operation to isolate individual fibril cross-sections, and then an ellipse was fit to each fibril cross-section. The minor diameter of the fit ellipse was taken to be the fibril diameter.

2.5. Mechanical testing and quantitative polarized light imaging

Tensile testing was performed to determine mechanical properties of $Fbln5^{+/+}$ and $Fbln5^{-/-}$ ATs and TBATs (n = 11–14/group). Prior to mechanical testing, the cross-sectional area (CSA) of the tendon samples was measured using a non-contact laser-scanning device. Tendons were then clamped into custom aluminum fixtures. To enhance gripping of the samples and provide sufficient gauge length, ATs were kept attached to the calcaneus, where the calcaneus was clamped directly and the free tendon end was clamped between pieces of sandpaper. The TBATs were removed from the medial cuneiform and clamped between pieces of sandpaper on both tendon ends. Verhoeff's stain was used to apply two lines perpendicular to the long axis of the tendons at approximately one third and two thirds distance along the gauge length to enable optical strain tracking. Subsequently, the fixtures with the clamped tendons were loaded into a mechanical loading device and submerged in PBS to maintain hydration. A pre-load of 0.1 N was applied and then samples were subjected to ten cycles to 3% clamp strain at 1 Hz to precondition the tissue. Following preconditioning, tendons were ramped to 5% clamp strain at a rate of 15% strain per second and held for five minutes before returning to the initial gauge length to evaluate stress relaxation. Lastly, tendons were subjected to triangular waveforms to 2%, 4%, and 8% clamp strain at 1% per second, which approximately correspond to the toe, transition, and linear regions of the loading curve. One minute of rest at the initial gauge length between each portion of the test was included to allow for partial tissue recovery. A custom quantitative polarized light imaging (QPLI) system was used to capture video of the entirety of the test to measure fiber alignment (York et al., 2014).

Tissue strain was determined by tracking the corners of the two stain lines within the video captured using the QPLI system, where the coordinates were used to calculate two-dimensional Lagrangian strain (Fang and Lake, 2015). Tissue stress was defined as the measured force divided by the initial CSA. Peak and equilibrium stress values were extracted from the stress relaxation data, where the equilibrium stress was taken as the average stress over the last 0.2 s of the stress relaxation test. Percent relaxation calculated as the percent difference between peak and equilibrium stresses. Hysteresis, or the percent energy lost during unloading, was calculated from the loading and unloading force-displacement curves to 2%, 4%, and 8% clamp strain. In addition, bilinear curve fitting was performed on the stress-strain loading curve to 8% clamp strain to determine toe modulus, linear modulus, and the stress and strain at the transition point (Lake et al., 2009).

Quantitative collagen alignment was determined using data collected using the QPLI system (Eekhoff et al., 2017; York et al., 2014). A region of interest was created between the two stain lines on each tendon surface; all pixels within the region of interest were analyzed for each frame of the video. Two independent measures were taken from these data: the average degree of polarization (AVG DoLP) and the standard deviation of the angle of polarization (STD AoP), which correspond to the strength of collagen alignment and (inversely) to the uniformity of collagen alignment within the sample, respectively. The AVG DoLP and STD AoP values immediately preceding stress relaxation (pre-SR), at the onset of stress relaxation (peak), at the end of stress relaxation (equilibrium), immediately following stress relaxation (post-SR), immediately preceding the ramp to 8% clamp strain (zero), at the calculated transition strain during the ramp to 8% clamp strain

(transition), and at double the calculated transition strain during the ramp to 8% clamp strain (linear) were extracted to make comparisons between genotypes.

2.6. Data analysis

Two-photon microscopy image stacks and transmission electron images were assessed qualitatively for the amount and quality of elastic fibers visible within the midsubstance of the tendon. A statistical comparison was not made for collagen fibril diameters due to low sample size, but the distributions were qualitatively compared between genotypes and between tendons. All compositional and mechanical data were analyzed using a two-way analysis of variance (ANOVA), where the two factors were genotype (i.e., $Fbln5^{-/-}$ vs. $Fbln5^{+/+}$) and tendon type (i.e., AT vs. TBAT). QPLI data were analyzed using two-way repeated measures ANOVA with factors of genotype and test region and with Greenhouse-Geisser corrections to account for lack of sphericity in the data. Bonferroni post-hoc tests were performed to determine the significance of differences between individual means; p-values less than 0.05 were considered significant and p-values less than 0.10 were considered to be trending towards significance.

3. Results

3.1. Compositional analysis

Biochemical analysis demonstrated subtle differences between the AT and TBAT and no differences between genotypes (Fig. 1). Collagen content was 18% greater in ATs compared to TBATs ($p = 0.001$). Similarly, desmosine content was 16% greater in ATs, although this effect did not reach statistical significance ($p = 0.054$). The ratio between desmosine and collagen was similar for all tendons analyzed.

Likewise, collagen cross-linking was unaffected by genotype, but the TBAT was more heavily cross-linked than the AT (Fig. 2). The amount of the mature cross-link HP was 53% greater in TBATs compared to ATs (Fig. 2(a)), while LP content was below detectable levels (not shown). Immature cross-links were more similar across tendon types, with 25% more DHLNL in the TBAT (Fig. 2(b)) and no significant difference in HLNL (Fig. 2(c)).

3.2. Two-photon microscopy

Optical clearing with fructose enabled deep two-photon imaging. Collagen appeared normal in each sample: densely packed and highly aligned fibers with regions of periodic crimp were visible throughout the tendons (Fig. 3). No differences in collagen structure were noted between genotypes or between tendon types. In $Fbln5^{+/+}$ ATs and TBATs, elastic fibers were long, thin, and sparsely distributed (Fig. 3(a,c)). Single elastic fibers could often be seen spanning across the entire field of view (509 μm). Some branching of elastic fibers was observed, although most fibers appeared disconnected from other fibers. Within $Fbln5^{+/+}$ samples, elastic fibers appeared to be more numerous in ATs compared to TBATs (Fig. 3(e and f)). Conversely, no distinct elastic fibers were discernible in $Fbln5^{-/-}$ ATs and TBATs, indicating a lack of

distinct autofluorescent signal from elastin in these tissues (Fig. 3(b,d)). Analysis of elastin volume from segmented images demonstrated a significant effect of genotype (Fig. 3(g)). While this measure of elastin volume was greater in $Fbln5^{+/+}$ ATs compared to TBATs, the tendon-type comparison did not reach statistical significance.

3.3. Transmission electron microscopy

Elastic fibers were located and imaged in both ATs and TBATs using TEM (Fig. 4). A total of 232 images were acquired from the eight samples prepared for TEM. The elastic fiber components discernible from the images were microfibrils (~10–12 nm diameter cylinders) and elastin (dark amorphous staining within bundles of microfibrils). In $Fbln5^{+/+}$ samples, groups of small, distinct microfibrils formed a scaffold for elastin, which was generally located within the center of the group of microfibrils (e.g., Fig. 4(a,n)). Organized, connected elastin was present with most groups of microfibrils in both $Fbln5^{+/+}$ ATs and TBATs. Still, there were also groups of microfibrils where no elastin was present (e.g., Fig. 4(i and j)); these structures are often referred to as oxytalan fibers (Montes, 1996; Caldini et al., 1990). Elastic and oxytalan fibers were sparsely dispersed throughout the whole tendon, and no obvious regional differences in fiber density were noted within the sections. Some elastic and oxytalan fibers were present directly adjacent to cells (e.g., Fig. 4(e and f)), while others were far from any cell and situated between collagen fibrils (e.g., Fig. 4(a and b)). While the cross-sections of most fibers were roughly circular, others appeared to have elongated or irregularly shaped cross-sections (e.g., Fig. 4(e,g)). On average, elastic fibers in ATs appeared to contain more elastin than those in TBATs, although there was a range of visible elastin content in both tendons. Most elastic fibers were aligned with the dominant direction of the collagen fibrils, although some fibers were seen at a slight angle from the dominant collagen orientation (e.g., Fig. 4(o)).

The structure of the fibrillin microfibrils appeared unaltered in $Fbln5^{-/-}$ ATs and TBATs (e.g., Fig. 4(c and d)). However, there was a clear lack of organized elastin. In the majority of images, no elastin could be identified. Where elastin was present, it appeared to be globular and disconnected (e.g., Fig. 4(p,q)). No elastic fibers with an organized and connected elastin core were observed in either $Fbln5^{-/-}$ ATs or TBATs. Outside of elastin organization, no obvious qualitative differences in collagen fibrils, cells, or overall structure were noted in tendons from $Fbln5^{-/-}$ mice compared to $Fbln5^{+/+}$ controls. Quantification of fibril diameters showed that ATs contained larger fibrils compared to TBATs, yet there was no noticeable effect of genotype on collagen fibril distribution for either tendon (Fig. 5).

3.4. Mechanical testing and quantitative polarized light imaging

Tendon CSA was not affected by genotype but significantly differed between tendon type. The least squares mean of the CSA for the AT and TBAT was 0.232 mm^2 and 0.093 mm^2, respectively (data not shown).

Both peak and equilibrium stresses during stress relaxation were 22–23% greater in TBATs compared to ATs ($p = 0.033$ and $p = 0.029$, respectively), yet no significant genotype effect was observed (Fig. 6(b and c)). The mean percent relaxation was between 29 and 30% for all
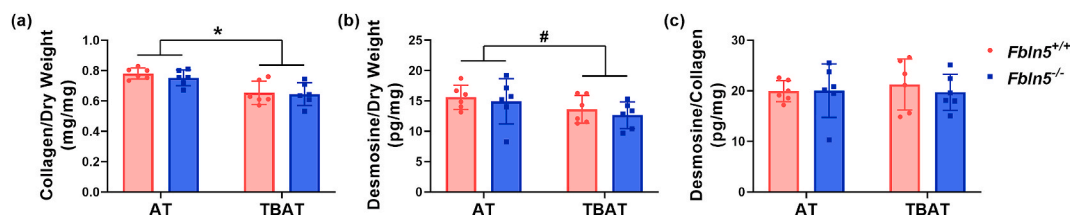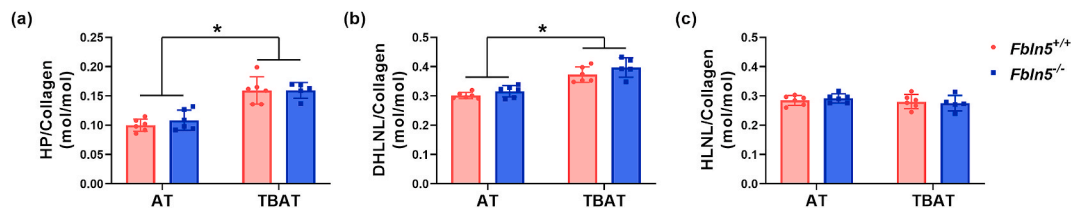

Fig. 1. (a) Collagen and (b) desmosine content were slightly lower in the TBAT compared to AT when normalized to dry weight, with no effect of genotype. (c) Desmosine to collagen ratio was unaffected by either tendon type or genotype. *$p < 0.05$. #$p < 0.10$.

Fig. 2. (a) HP and (b) DHLNL content were greater in the TBAT compared to the AT with no effect of genotype. (c) HLNL was unaffected by either tendon type of genotype. $*p < 0.05$.
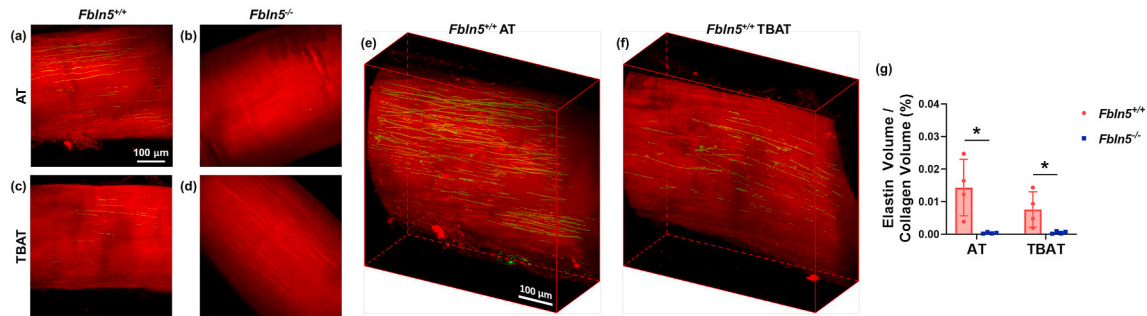
Fig. 3. Label-free two-photon microscopy images of optically cleared tendon samples. (a–d) Representative maximum intensity projections over a depth of 80 μm showing collagen (red) and elastin (green) in murine tendon. Sparsely distributed and aligned elastic fibers were visible in $Fbln5^{+/+}$ (a) ATs and (c) TBATs, while the elastin signal was absent in $Fbln5^{-/-}$ (b) ATs and (d) TBATS. Three-dimensional reconstructions of full-depth image stacks of a $Fbln5^{+/+}$ (e) AT and (f) TBAT. (g) Elastin volume in segmented image stacks was greater in $Fbln5^{+/+}$ tendons compared to $Fbln5^{-/-}$ tendons. $*p < 0.05$.

groups and was unaffected by both genotype and tendon type (Fig. 6(d)).

Hysteresis values were similar between $Fbln5^{-/-}$ and $Fbln5^{+/+}$ tendons and generally increased with increasing strain, although some tendon type effects were noted (Fig. 6(e–h)). At 2% and 4% strain the TBATs experienced greater hysteresis than ATs, while at 8% ATs experienced greater hysteresis than TBATs. This reversed effect at 8% strain is likely due to many of the AT samples nearing or surpassing the yield point at 8% strain, indicated by a noticeable inflection in the loading curve (Supplemental Fig. S1), while the TBATs showed no indication of yielding prior to 8% strain. Three out of thirteen $Fbln5^{+/+}$ ATs and two out of eleven $Fbln5^{-/-}$ ATs failed at the enthesis before reaching 8% strain, and consequently these samples were excluded from analysis of hysteresis at 8% strain. No TBATs failed during mechanical testing.

Bilinear fitting of the stress-strain curve to 8% clamp strain yielded a tendon-specific effect of genotype on linear modulus (Fig. 6(i–m), Fig. 7). While the toe modulus, transition strain, and transition stress were similar between each group, the mean linear modulus was 47% greater in $Fbln5^{-/-}$ ATs at 656 MPa compared to $Fbln5^{+/+}$ ATs at 446 MPa, but was unaffected by genotype in TBATs where the least squares mean of the linear modulus across both genotypes was 673 MPa (interaction effect $p = 0.043$).

Collagen alignment metrics (i.e., AVG DoLP and STD AoP) were similar between genotypes throughout the test for both tendons (Fig. 8). However, while specific values were similar, the $Fbln5^{-/-}$ ATs experienced greater changes in alignment during stress relaxation compared to $Fbln5^{+/+}$ ATs (Fig. 8(b and c)), as indicated by significant interaction effects between genotype and test region for both AVG DoLP and STD AoP ($p = 0.027$ and $p = 0.045$, respectively). These interaction effects were specific to ATs; TBATs had no significant interaction or genotype effects on alignment during stress relaxation (Fig. 8(d and e)). During the ramp to 8% strain, AVG DoLP generally increased and STD AoP generally decreased for both tendons with increasing strain, but no interaction or genotype effects were noted during this ramp (Fig. 8(f–j)).

4. Discussion

The key result from this study is that malformed elastic fibers in

tendon caused a tendon-specific increase in linear modulus (Fig. 6(m)). In agreement with our hypothesis, the AT was affected to a greater extent than the TBAT; however, it was unexpected that the TBAT displayed no effects of genotype on mechanical properties. The greater desmosine content in the AT may partially account for this tendon-specific effect, but the difference in desmosine quantity was small and unlikely to fully account for the data (Fig. 1(b)). Therefore, it appears that elastic fibers may play a more mechanical role in the AT compared to their contribution in the TBAT. This observation corresponds well with the functional requirements of the two tendons, where the AT is typically subjected to more high magnitude cyclic strain compared to the TBAT during *in vivo* use (Alexander, 1991). Moreover, many of the mechanical differences between $Fbln5^{+/+}$ ATs and TBATs, such as a reduced linear modulus and lower hysteresis within the working range of the tendon, are similar to those seen between the equine SDFT and CDET (Batson et al., 2010; Thorpe et al., 2013). However, while the energy-storing murine AT had less collagen cross-linking than the positional TBAT, previous studies have reported greater collagen cross-linking in the energy-storing equine and bovine SDFT compared to the positional CDET (Thorpe et al., 2010; Herod et al., 2016). Consequently, meaningful comparisons are possible between these structurally dissimilar models but still must be exercised with caution regarding the structural and compositional dissimilarities. Both models should be studied in concert; the murine tendon used in the current study reveals information regarding the role of fascicular elastic fibers, while larger tendons containing IFM are necessary to determine the distinct role of interfascicular elastic fibers in tendon.

The increase in linear modulus of $Fbln5^{-/-}$ ATs was caused by a change in the structure of elastic fibers but not overall composition of the tendon. Desmosine, collagen, and immature and mature collagen cross-link content were all unaffected by genotype in this model (Figs. 1 and 2). The structure of collagen, imaged with both two-photon microscopy and transmission electron microscopy, appeared identical between the $Fbln5^{+/+}$ and $Fbln5^{-/-}$ tendons. In contrast, the elastic fiber structure was clearly disrupted. Disconnected elastin globules were found in close proximity to microfibrils in transmission electron micrographs of $Fbln5^{-/-}$ tendons, in place of the long, organized core of
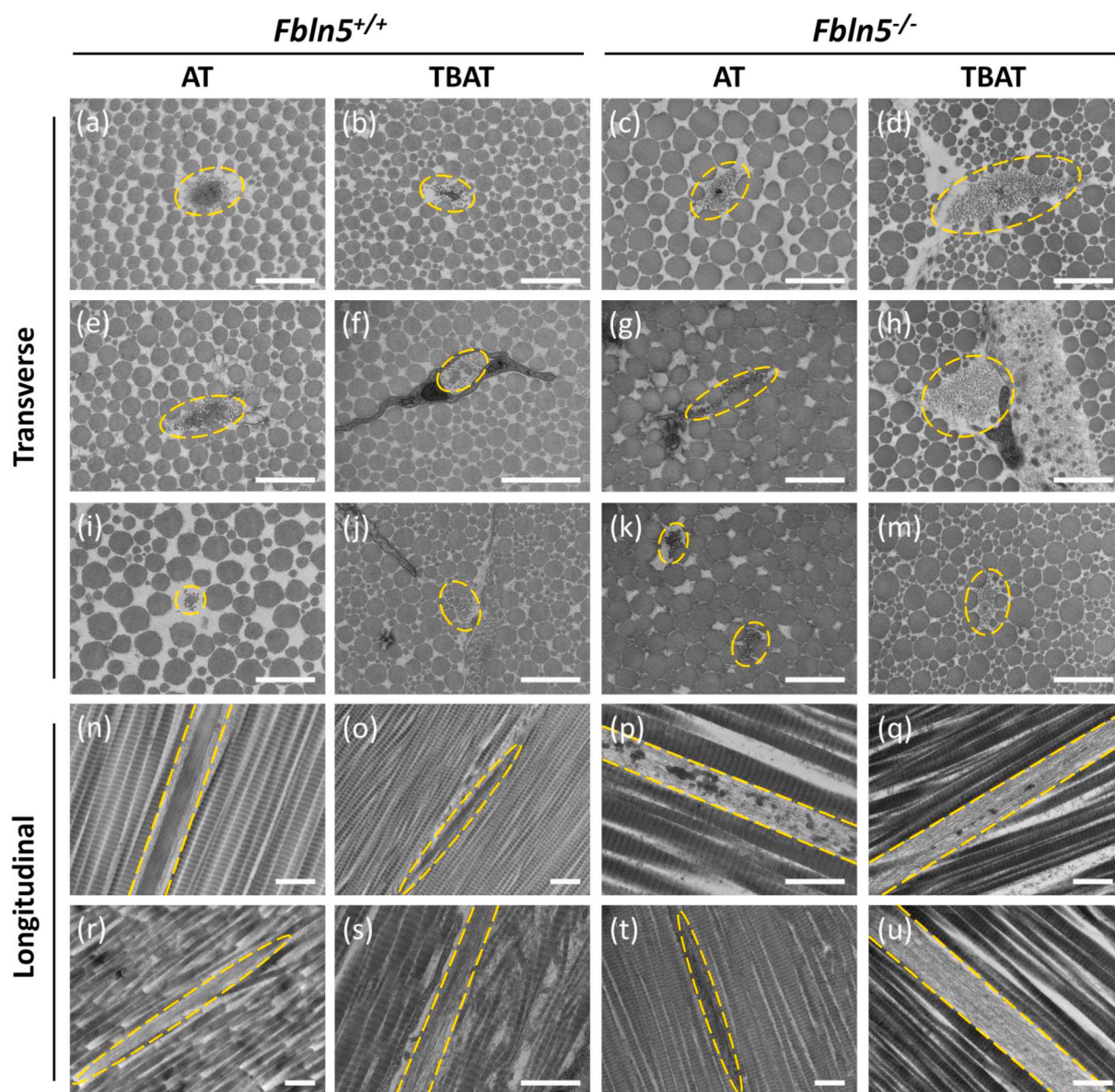
Fig. 4. Transverse and longitudinal transmission electron micrographs of *Fbln5*$^{+/+}$ and *Fbln5*$^{-/-}$ ATs and TBATs. Elastic/oxytalan fibers are outlined with dashed yellow lines. Elastic fibers in *Fbln5*$^{+/+}$ tendons contained an organized core of elastin, while elastic fibers in *Fbln5*$^{-/-}$ tendons demonstrated disconnected elastin globules. Some elastic fibers were located near cells as part of the pericellular matrix in both genotypes. Scale bar = 500 nm.
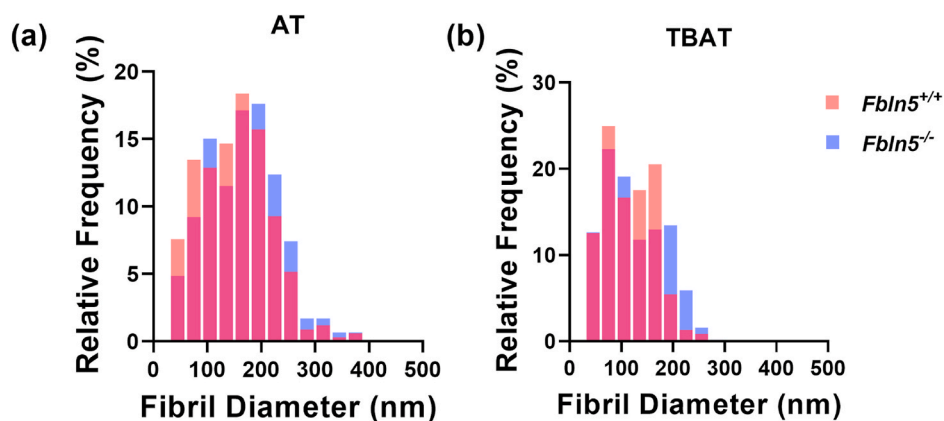

Fig. 5. Distributions of collagen fibril diameters in (a) *Fbln5*$^{+/+}$ and *Fbln5*$^{-/-}$ ATs and (b) *Fbln5*$^{+/+}$ and *Fbln5*$^{-/-}$ TBATs. Distributions appeared similar between genotypes while ATs tendons tended to contain more larger diameter fibrils. Statistical comparisons between groups were not made due to small sample sizes.
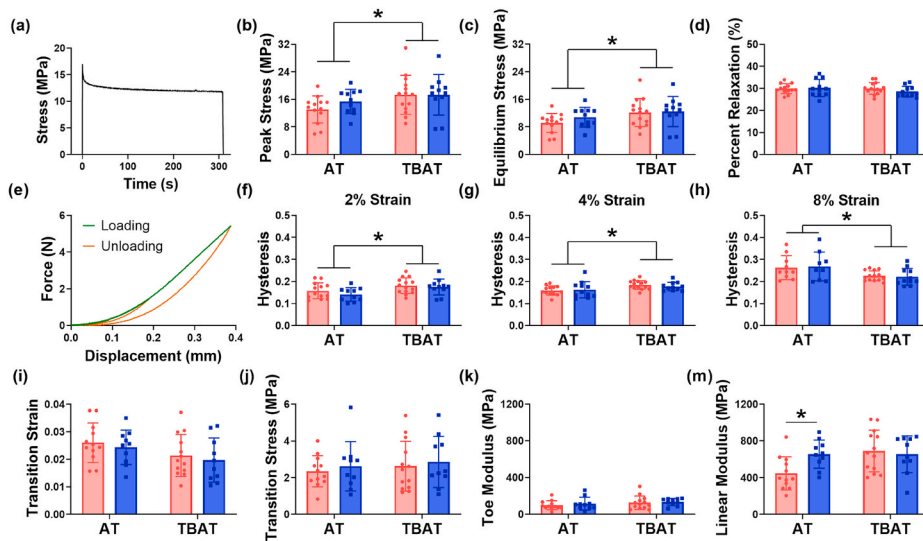
Fig. 6. Mechanical properties of $Fbln5^{+/+}$ and $Fbln5^{-/-}$ ATs and TBATs. (a) Representative stress relaxation curve from a $Fbln5^{+/+}$ AT. (b) Peak and (c) equilibrium stress were greater in TBATs compared to ATs with no effect of genotype, while (d) percent relaxation was unaffected by either tendon type or genotype. (e) Representative loading and unloading curves to 2%, 4%, and 8% clamp stain from a $Fbln5^{+/+}$ AT. Hysteresis at (f) 2% and (g) 4% strain was greater in TBATs compared to ATs, while hysteresis at (h) 8% strain was greater in ATs compared to TBATs. Hysteresis at all strain magnitudes was unaffected by genotype. (i) Transition strain, (j) transition stress, and (k) toe modulus were all unaffected by both genotype and tendon type. (m) Fibulin-5 deficiency affected linear modulus of ATs differently than TBATs (interaction effect $p = 0.043$). $Fbln5^{-/-}$ ATs has a greater linear modulus compared to $Fbln5^{+/+}$ ATs, while TBATs were unaffected by genotype. $*p < 0.05$.
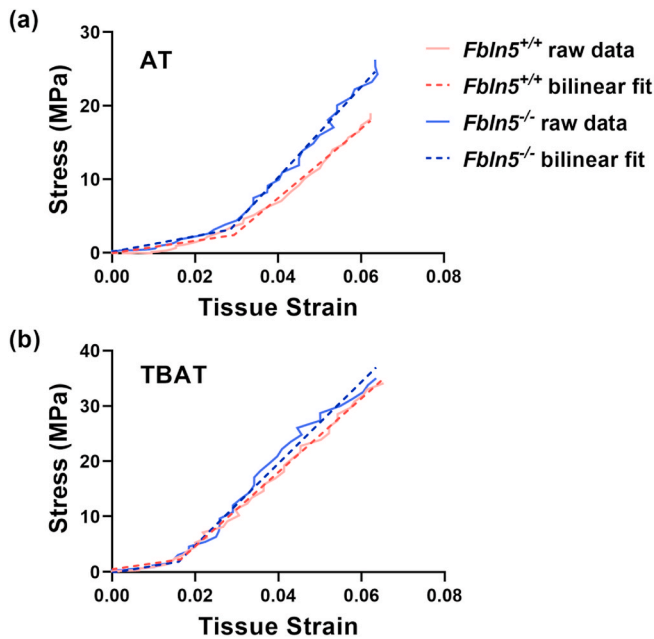

Fig. 7. Representative stress-strain loading curves of $Fbln5^{+/+}$ and $Fbln5^{-/-}$ (a) ATs and (b) TBATs with corresponding bilinear curve fits. The larger linear modulus in the $Fbln5^{-/-}$ AT compared to the $Fbln5^{+/+}$ AT can be seen as a greater slope in the stress-strain curve past the transition point where the bilinear fit lines intersect.

elastin found in elastic fibers of $Fbln5^{+/+}$ tendons (Fig. 4). Additionally, the two-photon excited autofluorescent signal from elastic fibers was indiscernible from the background noise (Fig. 3). This lack of signal was not a result of the absence of elastin, as indicated by the presence of elastin in compositional analysis and TEM. Rather, the elastin that was present in the $Fbln5^{-/-}$ tendons did not emit the same signal that was observed in $Fbln5^{+/+}$ tendons because of its improper assembly. While our biochemistry data indicated no effect of genotype on desmosine content, isodesmosine or immature elastin cross-links could have been affected. Additionally, although equal desmosine content strongly suggests equal elastin content between genotypes, it is possible in theory that the ratio of desmosine to elastin was altered and consequently the elastin content would vary correspondingly. In summary, elastic fibers

in $Fbln5^{-/-}$ tendons clearly demonstrated irregular structure which appears to have led to the corresponding increase in linear modulus in the AT.

Results in the present study agree with our prior work in elastin haploinsufficient mice, which demonstrated a slight increase in linear stiffness of both ATs and supraspinatus tendons as a result of partial elastin deficiency (Eekhoff et al., 2017). The work with murine models can be contrasted by prior research which utilized elastase to degrade elastic fibers to determine the role in mechanical properties of tendon and ligament. Generally, these studies have reported decreased stresses in elastase treated tendon, resulting from either an elongated toe region or from a decreased modulus (Henninger et al., 2013; Fang and Lake, 2016; Grant et al., 2015). The main contributor to the contrasting results between these studies is the different way in which elastic fibers are removed or rendered nonfunctional. In genetically modified murine models, elastic fibers are never formed properly and the tendon grows and develops in the absence of elastic fibers; conversely, elastase-treated tendon develops under standard conditions only to have the elastic fibers degraded during the experiment. In other words, murine models investigate the outcome of tendons developing without proper elastic fibers, while elastase experiments investigate the specific contribution of elastic fibers in otherwise normal tendon. The main advantage of experiments using elastase is the starting point with healthy tendon that contains a normal elastic fiber network. However, elastase can target proteins other than elastin which may confound the results of these experiments, and the approach can only be used for post-mortem testing. Murine models overcome the non-specificity of elastase treatments and could be used to investigate the effects of a disturbed elastic fiber network in *in vivo* studies, although the disadvantage is the difficulty in uncoupling potential compensatory mechanisms from the effects of altered elastic fibers. In this study, this concern was alleviated by confirming the lack of differences in the collagen quantity and structure between genotypes, although it remains possible that other minor compensatory effects may have occurred.

The greater change in collagen alignment experienced by $Fbln5^{-/-}$ ATs during stress relaxation may be linked to the mechanisms causing the greater linear modulus of these tendons. If elastic fibers serve as linking components between adjacent bundles of collagen and regulate structural reorganization during loading, then the absence of fully functioning elastic fibers would increase strain-induced structural reorganization in tendon because a reduction in linking components would enable freer collagen movement. A similar effect on collagen
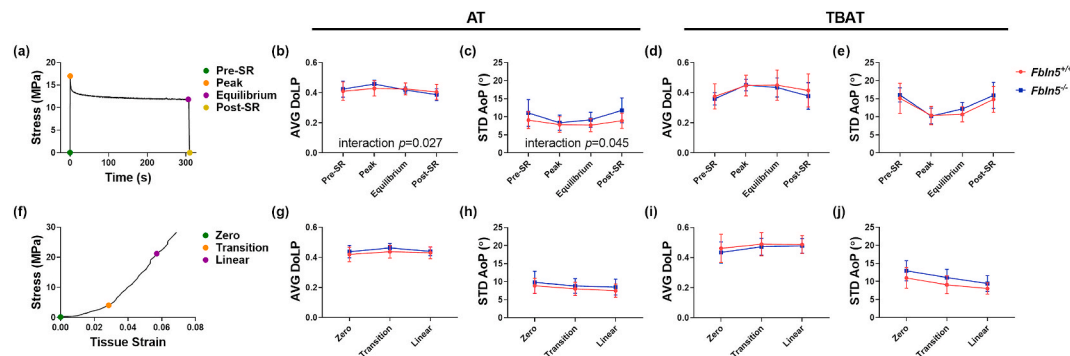
Fig. 8. QPLI data during stress relaxation and loading to 8% clamp strain. (a) AVG DoLP and STD AoP were recorded at pre-SR, peak, equilibrium, and post-SR points during the stress relaxation response. While values remained similar, $Fbln5^{-/-}$ ATs experienced greater changes to (b) AVG DoLP and (c) STD AoP during stress relaxation compared to $Fbln5^{+/+}$ ATs (interaction effect $p = 0.027$ and $p = 0.045$, respectively). (d,e) The AVG DoLP and STD AoP of $Fbln5^{+/+}$ and $Fbln5^{-/-}$ TBATs experienced changes throughout stress relaxation but no interaction or genotype effects were significant. (f) AVG DoLP and STD AoP were also recorded at zero, transition, and linear points during the ramp to 8% clamp strain. (g,i) AVG DoLP generally increased and (h,j) STD AoP generally decreased with increasing strain for $Fbln5^{+/+}$ and $Fbln5^{-/-}$ ATs and TBATs, yet no significant genotype or interaction effects were noted during loading to 8% clamp strain.

alignment measured using QPLI was noted in elastin haploinsufficient ATs (Eekhoff et al., 2017). However, the effect on changes in alignment in $Fbln5^{-/-}$ ATs was subtle and was confined to the stress relaxation portion of the test, which does not correspond to the measured change in linear modulus. It is possible that the tendons did not fully recover their initial structure after stress relaxation, and therefore structural changes which occurred during stress relaxation affected later parts of the test (Lee and Elliott, 2019b). Furthermore, the collagen alignment measurement using QPLI is limited to measuring the degree and uniformity of alignment at a length scale resolved using the camera macro lens (~10 μm/superpixel) and does not measure sliding between collagen bundles, which does not change overall alignment, or smaller scale structural reorganization. Consequently, additional changes to strain-induced structural reorganization may have been missed during other parts of the test. Imaging at a higher resolution during mechanical testing with a modality that could directly visualize collagen movement (e.g., two-photon microscopy) could identify smaller-scale collagen sliding and reorganization in future experiments (Fang and Lake, 2015; Szczesny and Elliott, 2014).

While an increase in linear modulus resulting from decreased integrity of a structural component of the ECM may seem counterintuitive, this again is a result of the role of elastic fibers as a linking component in tendon. The total content of elastin in tendon is low and therefore does not directly bear significant load as an individual component apart from the greater network of ECM, but instead regulates how collagen as the main structural component reacts to load. Without organized elastic fibers to regulate lateral interactions between bundles, the collagen is able to engage more fully and cause the tendon as a whole to stiffen. Perhaps stiffer linking components, such as interweaving small diameter collagen fibrils, compensate in the absence of proper elastic fibers to create a more rigid tendon after crimp has been extinguished in the toe region (Szczesny et al., 2017; Safa et al., 2019). Moreover, greater collagen engagement could possibly also result in greater accumulation of microdamage with repeated loading. This proposed phenomenon can be related to elastin-rich aortae, where the collagenous adventitia becomes more engaged when the elastic lamellae are disrupted, causing a decrease in compliance and distensibility (Yanagisawa and Wagenseil, 2019; Wagenseil et al., 2005; Le et al., 2014; Bellini et al., 2017). Similar changes to mechanical properties were also seen in inflation-extension testing of elastase-treated murine vaginal wall (Akintunde et al., 2018).

There are a number of limitations associated with this study. Fibulin-5 has secondary roles outside of elastic fiber assembly, such as regulation of matrix metalloproteinases (MMPs) (Tu et al., 2014; Budatha et al., 2013). While no changes to ECM structure or composition were observed other than disorganized elastic fibers, MMP dysregulation may have caused changes to less abundant matrix components, such as the minor collagens. Similarly, there may have been developmental compensation as an attempt to correct the functional limitations of malformed elastic fibers in the $Fbln5^{-/-}$ mice. However, no differences were detected in collagenous ECM of the tendon, suggesting any compensation effects were minimal compared to the effect of perturbed elastic fibers (Figs. 1(a) and 5). Finally, while the elastic fibers were severely malformed in $Fbln5^{-/-}$ tissue, they do still retain some function because the mice do not exhibit the same perinatal lethality as mice with systemic elastin knockout (Li et al., 1998). Therefore, the remaining capacity of the elastic fibers may have diminished or partially masked measured changes to mechanical properties. Future work could investigate in what capacity the malformed elastic fibers are still able to maintain some function.

Results of this study add to the growing collection of work demonstrating a significant role of elastic fibers in tendon mechanics. However, the bulk of work completed on this topic to date, current study included, are descriptive and are merely able to provide conjecture for how elastic fibers function within tendon. Further research incorporating more direct, mechanistic studies are necessary to elucidate the causes behind the observed altered mechanical properties in tendons with perturbed elastic fibers. This information ultimately could aid the maintenance or restoration of healthy tendon function in aging individuals and in patients with cutis laxa or other elastinopathic conditions.

Author statement

Jeremy D. Eekhoff: Conceptualization, Methodology, Formal analysis, Investigation, Writing – Original Draft. **Heiko Steenbock:** Investigation. **Ian M. Berke:** Methodology, Writing – Review & Editing. **Jürgen Brinckmann:** Resources, Writing – Review & Editing. **Hiromi Yanagisawa:** Resources, Writing – Review & Editing. **Jessica E. Wagenseil:** Resources, Writing – Review & Editing. **Spencer P. Lake:** Conceptualization, Writing – Review & Editing, Supervision.

Declaration of competing interest

The authors declare that they have no known competing financial interests or personal relationships that could have appeared to influence the work reported in this paper.

and image interpretation during the course of this study.

Appendix A. Supplementary data

Supplementary data to this article can be found online at https://doi.org/10.1016/j.jmbbm.2020.104134.

Funding

References

Akintunde, A.R., Robison, K.M., Capone, D.J., Desrosiers, L., Knoepp, L.R., Miller, K.S., 2018. Effects of elastase digestion on the murine vaginal wall biaxial mechanical response. J. Biomech. Eng. 141, 021011 https://doi.org/10.1115/1.4042014.

Alexander, R.M., 1991. Energy-saving mechanisms in walking and running. J. Exp. Biol. 160, 55–69.

Avery, N.C., Sims, T.J., Bailey, A.J., 2009. Quantitative determination of collagen cross-links. In: Even-Ram, S., Artym, V. (Eds.), Extracell. Matrix Protoc, second ed. Humana Press, pp. 103–121.

Baldwin, A.K., Simpson, A., Steer, R., Cain, S.A., Kielty, C.M., 2013. Elastic fibres in health and disease. Expet Rev. Mol. Med. 15, 1–30. https://doi.org/10.1017/erm.2013.9.

Batson, E.L., Paramour, R.J., Smith, T.J., Birch, H.L., Patterson-Kane, J.C., Goodship, A. E., 2010. Are the material properties and matrix composition of equine flexor and extensor tendons determined by their functions? Equine Vet. J. 35, 314–318. https://doi.org/10.2746/042516403776148327.

Bellini, C., Bersi, M.R., Caulk, A.W., Ferruzzi, J., Milewicz, D.M., Ramirez, F., et al., 2017. Comparison of 10 murine models reveals a distinct biomechanical phenotype in thoracic aortic aneurysms. J. R. Soc. Interface 14, 20161036. https://doi.org/10.1098/rsif.2016.1036.

Berk, D.R., Bentley, D.D., Bayliss, S.J., Lind, A., Urban, Z., 2012. Cutis laxa: a review. J. Am. Acad. Dermatol. 66, 842. https://doi.org/10.1016/j.jaad.2011.01.004 e1-842.e17.

Budatha, M., Roshanravan, S., Zheng, Q., Weislander, C., Chapman, S.L., Davis, E.C., et al., 2011. Extracellular matrix proteases contribute to progression of pelvic organ prolapse in mice and humans. J. Clin. Invest. 121, 2048–2059. https://doi.org/10.1172/JCI45636.

Budatha, M., Silva, S., Montoya, T.I., Suzuki, A., Shah-Simpson, S., Wieslander, C.K., et al., 2013. Dysregulation of protease and protease inhibitors in a mouse model of human pelvic organ prolapse. PloS One 8. https://doi.org/10.1371/journal.pone.0056376.

Caldini, E.G., Caldini, N., De-Pasquale, V., Strocchi, R., Guizzardi, S., Ruggeri, A., et al., 1990. Distribution of elastic system fibres in the rat tail tendon and its associated sheaths. Cells Tissues Organs 139, 341–348. https://doi.org/10.1159/000147022.

Choi, J., Bergdahl, A., Zheng, Q., Starcher, B., Yanagisawa, H., Davis, E.C., 2009. Analysis of dermal elastic fibers in the absence of fibulin-5 reveals potential roles for fibulin-5 in elastic fiber assembly. Matrix Biol. 28, 211–220. https://doi.org/10.1016/j.matbio.2009.03.004.

Drewes, P.G., Yanagisawa, H., Starcher, B., Hornstra, I., Csiszar, K., Marinis, S.I., et al., 2007. Pelvic organ prolapse in fibulin-5 knockout mice: pregnancy-induced changes in elastic fiber homeostasis in mouse vagina. Am. J. Pathol. 170, 578–589. https://doi.org/10.2353/ajpath.2007.060662.

Dunham, C.L., Steenbock, H., Brinckmann, J., Reiter, A.J., Castile, R.M., Chamberlain, A. M., et al., 2020. Increased volume and collagen crosslinks drive soft tissue contribution to post-traumatic elbow contracture in an animal model. J. Orthop. Res. https://doi.org/10.1002/jor.24781 jor.24781.

Eekhoff, J.D., Fang, F., Kahan, L.G., Espinosa, G., Cocciolone, A.J., Wagenseil, J.E., et al., 2017. Functionally distinct tendons from elastin haploinsufficient mice exhibit mild stiffening and tendon-specific structural alteration. J. Biomech. Eng. 139, 111003. https://doi.org/10.1115/1.4037932.

Fang, F., Lake, S.P., 2015. Multiscale strain analysis of tendon subjected to shear and compression demonstrates strain attenuation, fiber sliding, and reorganization. J. Orthop. Res. 33, 1704–1712. https://doi.org/10.1002/jor.22955.

Fang, F., Lake, S.P., 2016. Multiscale mechanical integrity of human supraspinatus tendon in shear after elastin depletion. J. Mech. Behav. Biomed. Mater. 63, 443–455. https://doi.org/10.1016/j.jmbbm.2016.06.032.

Freeman, L.J., Lomas, A., Hodson, N., Sherratt, M.J., Mellody, K.T., Weiss, A.S., et al., 2005. Fibulin-5 interacts with fibrillin-1 molecules and microfibrils. Biochem. J. 388, 1–5. https://doi.org/10.1042/BJ20050368.

Godinho, M.S.C., Thorpe, C.T., Greenwald, S.E., Screen, H.R.C., 2017. Elastin is localised to the interfascicular matrix of energy storing tendons and becomes increasingly disorganised with ageing. Sci. Rep. 7, 9713. https://doi.org/10.1038/s41598-017-09995-4.

Gosline, J., Lillie, M., Carrington, E., Guerette, P., Ortlepp, C., Savage, K., 2002. Elastic proteins: biological roles and mechanical properties. Philos. Trans. R Soc. B Biol. Sci. 357, 121–132. https://doi.org/10.1098/rstb.2001.1022.

Grant, T.M., Thompson, M.S., Urban, J., Yu, J., 2013. Elastic fibres are broadly distributed in tendon and highly localized around tenocytes. J. Anat. 222, 573–579. https://doi.org/10.1111/joa.12048.

Grant, T.M., Yapp, C., Chen, Q., Czernuszka, J.T., Thompson, M.S., 2015. The mechanical, structural, and compositional changes of tendon exposed to elastase. Ann. Biomed. Eng. 43, 2477–2486. https://doi.org/10.1007/s10439-015-1308-5.

Henninger, H.B., Underwood, C.J., Romney, S.J., Davis, G.L., Weiss, J.A., 2013. Effect of elastin digestion on the quasi-static tensile response of medial collateral ligament. J. Orthop. Res. 31, 1226–1233. https://doi.org/10.1002/jor.22352.

Henninger, H.B., Valdez, W.R., Scott, S.A., Weiss, J.A., 2015. Elastin governs the mechanical response of medial collateral ligament under shear and transverse tensile loading. Acta Biomater. 25, 304–312. https://doi.org/10.1016/j.actbio.2015.07.011.

Herod, T.W., Chambers, N.C., Veres, S.P., 2016. Collagen fibrils in functionally distinct tendons have differing structural responses to tendon rupture and fatigue loading. Acta Biomater. 42, 296–307. https://doi.org/10.1016/j.actbio.2016.06.017.

Hill, J.R., Eekhoff, J.D., Brophy, R.H., Lake, S.P., 2020. Elastic fibers in orthopedics: form and function in tendons and ligaments, clinical implications, and future directions. J. Orthop. Res. https://doi.org/10.1002/jor.24695 jor.24695.

Holbrook, K.A., Byers, P.H., 1982. Structural abnormalities in the dermal collagen and elastic matrix from the skin of patients with inherited connective tissue disorders. J. Invest. Dermatol. 79, 7–16. https://doi.org/10.1038/jid.1982.3.

Hu, Q., Loeys, B.L., Coucke, P.J., De Paepe, A., Mecham, R.P., Choi, J., et al., 2006. Fibulin-5 mutations: mechanisms of impaired elastic fiber formation in recessive cutis laxa. Hum. Mol. Genet. 15, 3379–3386. https://doi.org/10.1093/hmg/ddl414.

Katsuta, Y., Ogura, Y., Iriyama, S., Goetinck, P.F., Klement, J.F., Uitto, J., et al., 2008. Fibulin-5 accelerates elastic fibre assembly in human skin fibroblasts. Exp. Dermatol. 17, 837–842. https://doi.org/10.1111/j.1600-0625.2008.00709.x.

Ke, M.T., Fujimoto, S., Imai, T., 2013. SeeDB: a simple and morphology-preserving optical clearing agent for neuronal circuit reconstruction. Nat. Neurosci. 16, 1154–1161. https://doi.org/10.1038/nn.3447.

Lake, S.P., Miller, K.S., Elliott, D.M., Soslowsky, L.J., 2009. Effect of fiber distribution and realignment on the nonlinear and inhomogeneous mechanical properties of human supraspinatus tendon under longitudinal tensile loading. J. Orthop. Res. 27, 1596–1602. https://doi.org/10.1002/jor.20938.

Le, V.P., Stoka, K.V., Yanagisawa, H., Wagenseil, J.E., 2014. Fibulin-5 null mice with decreased arterial compliance maintain normal systolic left ventricular function, but not diastolic function during maturation. Phys. Rep. 2, 1–16. https://doi.org/10.1002/phy2.257.

Lee, A.H., Elliott, D.M., 2019a. Comparative multi-scale hierarchical structure of the tail, plantaris, and Achilles tendons in the rat. J. Anat. 234, 252–262. https://doi.org/10.1111/joa.12913.

Lee, A.H., Elliott, D.M., 2019b. Multi - scale loading and damage mechanisms of plantaris and rat tail tendons. J. Orthop. Res. 37, 1827–1837. https://doi.org/10.1002/jor.24309.

Li, D.Y., Brooke, B., Davis, E.C., Mecham, R.P., Sorensen, L.K., Boak, B.B., et al., 1998. Elastin is an essential determinant of arterial morphogenesis. Nature 393, 276–280. https://doi.org/10.1038/30522.

Liu, X., Zhao, Y., Gao, J., Pawlyk, B., Starcher, B., Spencer, J.A., et al., 2004. Elastic fiber homeostasis requires lysyl oxidase-like 1 protein. Nat. Genet. 36, 178–182. https://doi.org/10.1038/ng1297.

Marchase, P., Holbrook, K., Pinnell, S.R., 1980. A familial cutis laxa syndrome with ultrastructural abnormalities of collagen and elastin. J. Invest. Dermatol. 75, 399–403. https://doi.org/10.1111/1523-1747.ep12523655.

Millesi, H., Reihsner, R., Hamilton, G., Mallinger, R., Menzel, E.J., 1995. Biomechanical properties of normal tendons, normal palmar aponeuroses and palmar aponeuroses from patients with dupuytren's disease subjected to elastase and chondroitinase treatment. Connect. Tissue Res. https://doi.org/10.3109/03008209509028398.

Montes, G.S., 1996. Structural biology of the fibres of the collagenous and elastic systems. Cell Biol. Int. 20, 15–27. https://doi.org/10.1006/cbir.1996.0004.

Nakamura, T., Lozano, P.R., Ikeda, Y., Iwanaga, Y., Hinek, A., Minamisawa, S., et al., 2002. Fibulin-5/DANCE is essential for elastogenesis in vivo. Nature 415, 171–175. https://doi.org/10.1038/415171a.

Pang, X., Wu, J.-P., Allison, G.T., Xu, J., Rubenson, J., Zheng, M.-H., et al., 2017. Three dimensional microstructural network of elastin, collagen, and cells in Achilles tendons. J. Orthop. Res. 35, 1203–1214. https://doi.org/10.1002/jor.23240.

Papke, C.L., Yanagisawa, H., 2014. Fibulin-4 and fibulin-5 in elastogenesis and beyond: insights from mouse and human studies. Matrix Biol. 37, 142–149. https://doi.org/10.1016/j.matbio.2014.02.004.

Safa, B.N., Peloquin, J.M., Natriello, J.R., Caplan, J.L., Elliott, D.M., 2019. Helical fibrillar microstructure of tendon using serial block-face scanning electron microscopy and a mechanical model for interfibrillar load transfer. J. R. Soc. Interface 16, 20190547. https://doi.org/10.1098/rsif.2019.0547.

Sakati, N.O., Nyhan, W.L., Shear, C.S., 1983. Syndrome of cutis laxa, ligamentous laxity, and delayed development. Pediatrics 72, 850–856.

Stoilov, I., Starcher, B.C., Mecham, R.P., Broekelmann, T.J., 2018. Measurement of elastin, collagen, and total protein levels in tissues. Methods Cell Biol. 143, 133–146. Elsevier Inc. first ed.

Szczesny, S.E., Elliott, D.M., 2014. Interfibrillar shear stress is the loading mechanism of collagen fibrils in tendon. Acta Biomater. 10, 2582–2590. https://doi.org/10.1016/j.actbio.2014.01.032.

Szczesny, S.E., Fetchko, K.L., Dodge, G.R., Elliott, D.M., 2017. Evidence that interfibrillar load transfer in tendon is supported by small diameter fibrils and not extrafibrillar tissue components. J. Orthop. Res. 35, 2127–2134. https://doi.org/10.1002/jor.23517.

Thorpe, C.T., Streeter, I., Pinchbeck, G.L., Goodship, A.E., Clegg, P.D., Birch, H.L., 2010. Aspartic acid racemization and collagen degradation markers reveal an accumulation of damage in tendon collagen that is enhanced with aging. J. Biol. Chem. 285, 15674–15681. https://doi.org/10.1074/jbc.M109.077503.

Thorpe, C.T., Udeze, C.P., Birch, H.L., Clegg, P.D., Screen, H.R.C., 2012. Specialization of tendon mechanical properties results from interfascicular differences. J. R. Soc. Interface 9, 3108–3117. https://doi.org/10.1098/rsif.2012.0362.

Thorpe, C.T., Klemt, C., Riley, G.P., Birch, H.L., Clegg, P.D., Screen, H.R.C., 2013. Helical sub-structures in energy-storing tendons provide a possible mechanism for efficient energy storage and return. Acta Biomater. 9, 7948–7956. https://doi.org/10.1016/j.actbio.2013.05.004.

Thorpe, C.T., Spiesz, E.M., Chaudhry, S., Screen, H.R.C., Clegg, P.D., 2015. Science in brief: recent advances into understanding tendon function and injury risk. Equine Vet. J. 47, 137–140. https://doi.org/10.1111/evj.12346.

Thorpe, C.T., Riley, G.P., Birch, H.L., Clegg, P.D., Screen, H.R.C.C., 2017. Fascicles and the interfascicular matrix show decreased fatigue life with ageing in energy storing tendons. Acta Biomater. 56, 58–64. https://doi.org/10.1016/j.actbio.2016.06.012.

Tu, K., Dou, C., Zheng, X., Li, C., Yang, W., Yao, Y., et al., 2014. Fibulin-5 inhibits hepatocellular carcinoma cell migration and invasion by down-regulating matrix metalloproteinase-7 expression. BMC Canc. 14, 1–9. https://doi.org/10.1186/1471-2407-14-938.

Wagenseil, J.E., Nerurkar, N.L., Knutsen, R.H., Okamoto, R.J., Li, D.Y., Mecham, R.P., et al., 2005. Effects of elastin haploinsufficiency on the mechanical behavior of mouse arteries. Am. J. Physiol. Heart Circ. Physiol. 289, 1209–1217. https://doi.org/10.1152/ajpheart.00046.2005.

Yanagisawa, H., Davis, E.C., 2010. Unraveling the mechanism of elastic fiber assembly: the roles of short fibulins. Int. J. Biochem. Cell Biol. 42, 1084–1093. https://doi.org/10.1016/j.biocel.2010.03.009.

Yanagisawa, H., Wagenseil, J., 2019. Elastic fibers and biomechanics of the aorta: insights from mouse studies. Matrix Biol. 1–13 https://doi.org/10.1016/j.matbio.2019.03.001.

Yanagisawa, H., Davis, E.C., Starcher, B.C., Ouchi, T., Yanagisawa, M., Richardson, J.A., et al., 2002. Fibulin-5 is an elastin-binding protein essential for elastic fibre development in vivo. Nature 415, 168–171. https://doi.org/10.1038/415168a.

Yanagisawa, H., Schluterman, M.K., Brekken, R.A., 2009. Fibulin-5, an integrin-binding matricellular protein: its function in development and disease. J. Cell Commun. Signal 3, 337–347. https://doi.org/10.1007/s12079-009-0065-3.

York, T., Kahan, L., Lake, S.P., Gruev, V., 2014. Real-time high-resolution measurement of collagen alignment in dynamically loaded soft tissue. J. Biomed. Optic. 19, 066011 https://doi.org/10.1117/1.JBO.19.6.066011.